BIOCHEMISTRY
including biophysical chemistry & molecular biology

Article

pubs.acs.org/biochemistry

Heme Binding Mechanism of Structurally Similar Iron-Regulated Surface Determinant Near Transporter Domains of *Staphylococcus aureus* Exhibiting Different Affinities for Heme

Yoshitaka Moriwaki,[*,†] Tohru Terada,[‡] Jose M. M. Caaveiro,[§] Yousuke Takaoka,[∥] Itaru Hamachi,[∥,⊥] Kouhei Tsumoto,[§,@,#] and Kentaro Shimizu[†]

[†]Department of Biotechnology and [‡]Agricultural Bioinformatics Research Unit, Graduate School of Agricultural and Life Sciences, The University of Tokyo, 1-1-1 Yayoi, Bunkyo-ku, Tokyo 113-8657, Japan

[§]Institute of Medical Sciences, The University of Tokyo, Tokyo 108-8639, Japan

[∥]Department of Synthetic Chemistry and Biological Chemistry, Kyoto University, Katsura, Nishikyo-Ku, Kyoto 615-8510, Japan

[⊥]Core Research for Evolutional Science and Technology (CREST), Japan Science and Technology Agency (JST), Sanbancho, Chiyoda-ku, Tokyo 102-0075, Japan

[@]Department of Bioengineering, Graduate School of Engineering, The University of Tokyo, 7-3-1 Hongo, Bunkyo-ku 113-8656, Japan

[#]Department of Medical Genome Science, School of Frontier Sciences, The University of Tokyo, Kashiwa 277-8562, Japan

Supporting Information

ABSTRACT: Near transporter (NEAT) domains of the iron-regulated surface determinant (Isd) proteins are essential for the import of nutritional heme from host animals to Gram-positive pathogens such as *Staphylococcus aureus*. The order of transfer of heme between NEAT domains occurs from IsdH to IsdA to IsdC, without any energy input despite the similarity of their three-dimensional structures. We measured the free energy of binding of heme and various metalloporphyrins to each NEAT domain and found that the affinity of heme and non-iron porphyrins for NEAT domains increased gradually in the same order as that for heme transfer. To gain insight into the atomistic mechanism for the differential affinities, we performed *in silico* molecular dynamics simulation and *in vitro* site-directed mutagenesis. The simulations revealed that the negatively charged residues that are abundant in the loop between strand β1b and the 3_{10} helix of IsdH-NEAT3 destabilize the interaction with the propionate group of heme. The higher affinity of IsdC was in part attributed to the formation of a salt bridge between its unique residue, Glu88, and the conserved Arg100 upon binding to heme. In addition, we found that Phe130 of IsdC makes the β7−β8 hairpin less flexible in the ligand-free form, which serves to reduce the magnitude of the entropy loss on binding to heme. We confirmed that substitution of these key residues of IsdC decreased its affinity for heme. Furthermore, IsdC mutants, whose affinities for heme were lower than those of IsdA, transferred heme back to IsdA. Thus, NEAT domains have evolved the characteristic residues on the common structural scaffold such that they exhibit different affinities for heme, thus promoting the efficient transfer of heme.

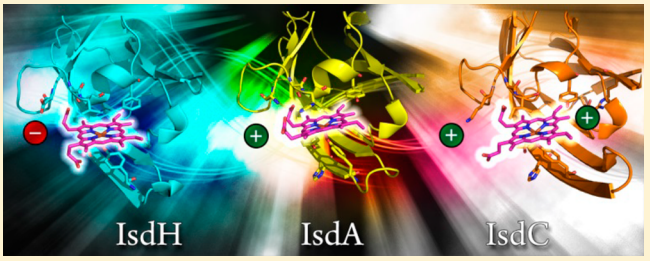

Acquisition of iron nutrients is essential for survival and proliferation of bacterial pathogens.[1−4] Although most mammalian host organisms, including humans, also have abundant iron, the amount of free iron is very limited because it has low solubility and is often chelated by heme and/or proteins (i.e., lactoferrin).[5,6] However, recent studies have revealed that *Staphylococcus aureus*, *Bacillus anthracis*, and other Gram-positive pathogens[7−9] have evolved the iron-regulated surface determinant (Isd) system to steal iron from the heme group of hemoglobin.[10−13] The Isd system is activated in response to iron depletion in the bacteria[10] and is composed of several proteins that extract, transport, and metabolize heme.[10,14−16]

The Isd proteins IsdH, IsdB, IsdA, and IsdC are anchored to the cell wall and display one or more copies of the Near transporter (NEAT) domain. IsdH-NEAT1 and -NEAT2 domains[17−19] and the IsdB-NEAT1[20] domain bind to hemoglobin (or haptoglobin−hemoglobin). IsdH-NEAT3 (IsdH-N3), IsdB-NEAT2 (IsdB-N2), IsdA-NEAT (IsdA-N), and IsdC-NEAT (IsdC-N) domains capture free heme extracted from hemoglobin and transfer it to downstream proteins. It is important to note that there are two main types

Received: June 27, 2013
Revised: November 17, 2013
Published: November 18, 2013

ACS Publications © 2013 American Chemical Society

dx.doi.org/10.1021/bi4008325 | *Biochemistry* 2013, 52, 8866−8877

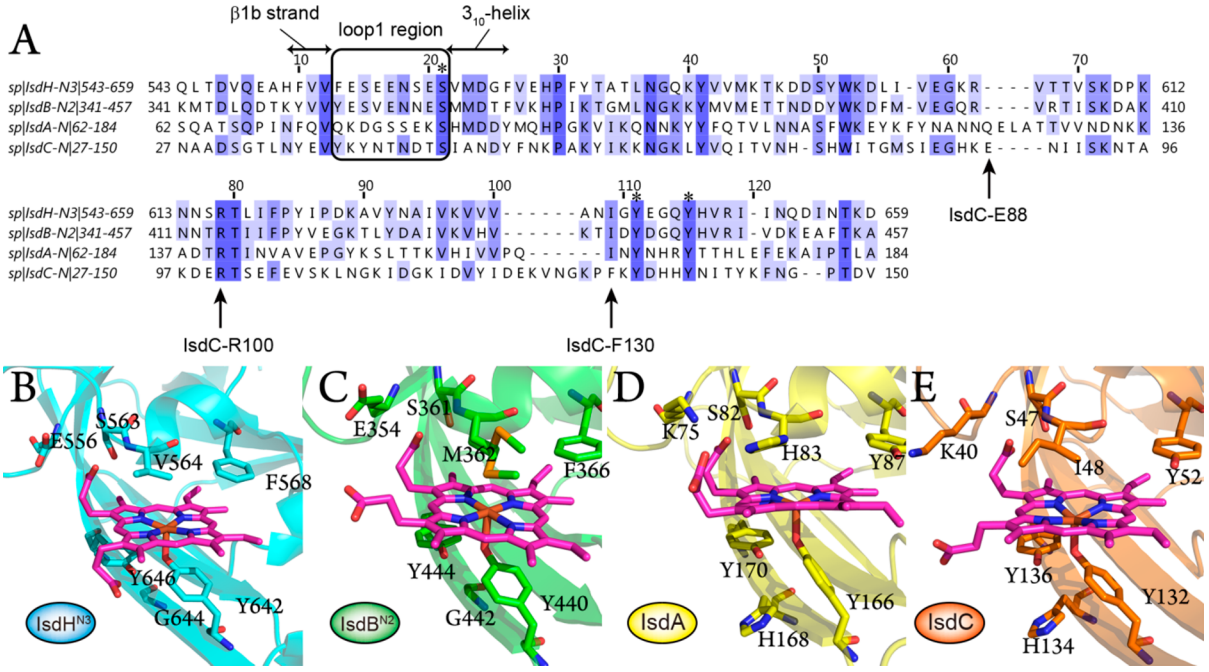

Figure 1. (A) Sequence alignments of heme-binding NEAT domains in *S. aureus*. All the regions of NEAT domains were annotated in UniProt. The alignment was generated using Jalview version 2.8[31] and the T-Coffee algorithm.[32] A black circle indicates the loop 1 region. (B−E) Arrangement of residues around the heme-binding pocket of IsdH-N3 (PDB entry 2Z6F), IsdB-N2 (PDB entry 3RUR), IsdA-N (PDB entry 2ITF), and IsdC-N (PDB entry 2O6P), respectively.

of NEAT domains: hemoglobin-binding and heme-transferring. Although they share a similar three-dimensional structure and are linked to each other in IsdH and IsdB, the first type binds hemoglobin and the second type binds heme.[19] For example, a recent study has shown that the IsdH-N2-N3 bidomain unit efficiently extracts heme from hemoglobin.[18] Given that the heme molecule thus extracted binds to the N3 part of the bidomain, the heme-transfer relay starts with IsdH-N3 (or IsdB-N2). IsdE, which is anchored in the plasma membrane along with IsdF, receives heme from IsdC and imports it into the cytoplasm.[21,22] Finally, IsdG and IsdI degrade heme to produce iron.[23−25]

IsdH and IsdB are located in the outermost region of the cell wall, whereas IsdA and IsdC are located in the middle and innermost regions of the cell wall, respectively. Heme transfer occurs effectively from IsdH-N3 to IsdA-N to IsdC-N or, alternatively, from IsdB-N2 to IsdA-N to IsdC-N.[26] Heme is transferred rapidly from upstream to downstream NEAT domains and between identical NEAT domains.[27−29] The efficient transfer of heme through the thick cell wall (20−80 nm in Gram-positive bacteria[30]) may be optimized by the sequential arrangement of the Isd proteins in the cell wall and by the rapid transfer of heme between NEAT domains.

The tertiary structures of the NEAT domains have revealed unique interactions between the NEAT domains and heme. In all the NEAT domains, the ferric iron atom of heme is coordinated by a conserved tyrosine residue, which is uncommon in most heme-binding proteins, in which a histidine residue coordinates iron (Figure 1).[33−36] In addition, a propionate group of heme forms hydrogen bonds with some of the surrounding residues (Figure 1). As downstream NEAT domains have a higher affinity for heme, an affinity-driven heme-transfer mechanism has been proposed.[34] However, as the structures of the NEAT domains are quite similar to each other, it is difficult to explain the physicochemical basis of the difference in affinity. The atomistic mechanism of heme transfer therefore remains unclear.

In this study, we used experimental and theoretical approaches to explore the dominant factor determining the direction of heme transfer between the NEAT domains. We also used non-iron metalloporphyrins to examine the role of metal ions in the transfer. We measured free energy changes upon binding of heme for IsdH-N3, IsdA-N, and IsdC-N and compared the values with theoretical calculations obtained by molecular dynamics (MD) simulations. We identified important residues for the efficient transfer of heme based on the results of these MD simulations. The theoretical predictions were verified experimentally using mutants and a chimera of the NEAT domains.

MATERIALS AND METHODS

Preparation of Metalloporphyrins and Isd Proteins. Hemin and Mn(III)-PPIX chloride were purchased from Frontier Scientific (Logan, UT). Ga(III)-PPIX hydroxide was synthesized according to the methodology of Nakae et al.[37]

As reported previously,[38] cloning, expression, and purification of heme-free (apo) proteins IsdH-N3 (comprising residues Gly-534−Gln-664) and full-length IsdA except for the N- and C-terminal signal sequences (residues Ala-47−Thr-316) were performed using *Escherichia coli* RP523,[39] a *hemB* mutant strain. IsdA-N (residues Ser-62−Ala-184) and full-length IsdC except for the N- and C-terminal signal sequences (residues Ala-28−Thr-192) were amplified by polymerase chain reaction and cloned into a pTAC-MAT-Tag-2 expression vector (Sigma-Aldrich, St. Louis, MO). Expression and purification were conducted as described above. The His_6 tag was always cleaved off with thrombin protease (Sigma-Aldrich).

Isothermal Titration Calorimetry (ITC) Analysis. Thermodynamic parameters of the interaction between the NEAT domains and metalloporphyrins were determined with

dx.doi.org/10.1021/bi4008325 | *Biochemistry* 2013, 52, 8866−8877

iTC 200 (GE Healthcare) at 25 °C. The apo form of IsdH-N3, IsdA-N, full-length IsdC, or full-length IsdC mutants were equilibrated with buffer [0.2 M NaCl and 50 mM Tris-HCl (pH 8.0)]. It is important to note that these protein samples did not contain heme derived from the expression system. Proteins filled in the calorimeter cell were diluted to a concentration of 20 μM with buffer containing 5% (v/v) dimethyl sulfoxide (DMSO). A solution of each metalloporphyrin with 5% (v/v) DMSO (375 μM) was prepared from powder for each experiment and filled into the calorimeter syringe. We also measured the affinity of IsdH-NEAT3 at 15, 20, and 30 °C to evaluate its temperature dependence. The binding isotherms were fit to a one-site binding model using ORIGIN version 7.0.

Heme Transfer between IsdH-N3 and IsdC Measured by UV−Visible Absorbance Spectroscopy. The transport of heme from IsdH-N3 to IsdC was measured according to the methodologies of Liu et al.[27] The holo form of IsdH-N3 (14 μM) and the apo form of IsdC (16 μM) were mixed in 1 mL of 50 mM sodium phosphate buffer (pH 7.3) for 1 or 2 min. The proteins were subsequently separated by ion-exchange chromatography using a diethylaminoethyl Sepharose (DEAE-Sepharose) column. IsdH-N3 binds to the column, whereas full-length IsdC appears in the flow-through eluate. IsdH-N3 was recovered with a solution containing 500 mM NaCl. To examine the transfer of metalloporphyrins, we measured the intensities of the Soret band [heme, 403 nm; Ga(III)-PPIX, 413 nm; Mn(III)-PPIX, 375 nm] for both IsdH-N3 and IsdC using a Jasco (Tokyo, Japan) spectrophotometer.

Construction of Initial Structures of MD Simulations. Crystal structures have been determined for heme-bound (holo) forms of IsdH-N3 (PDB entry 2Z6F), IsdA-N (PDB entry 2ITF), and IsdC-N (PDB entry 2O6P), and for heme-free (apo) forms of IsdH-N3 (PDB entry 2E7D) and IsdA-N (PDB entry 2ITE). Their coordinates were downloaded from the PDB and used as the initial structures of the MD simulations. As the crystal structure of the apo form of IsdC-N has not been determined, the structure of its apo form was constructed by deleting heme from its holo structure. The structure of a loop 1 chimera between IsdC-N and IsdH-N3 (IsdC-N-loop 1H) was modeled by superposing the Cα atoms of the holo structure of IsdC-N upon those of the holo structure of IsdH-N3 and by subsequently substituting the loop 1 region (residues Tyr-39−Thr-46) of IsdC-N for the corresponding region (Phe-555−Glu-562) of IsdH-N3 (Table S1 of the Supporting Information). The structure of the IsdC-N-F130A mutant was constructed using the "mutagenesis" function implemented in PyMOL.[40] The N- and C-termini of all the protein models were capped with an acetyl group and an *N*-methyl group, respectively. The protonation states of the histidine residues at pH 7.0 were determined by PROPKA3.[41] The deprotonated form was used for the tyrosine residues coordinating to the iron of heme (Y642 of IsdH-N3, Y166 of IsdA-N, and Y132 of IsdC-N), not only in the MD simulations of the holo forms but also for the apo forms because the MD simulation with the protonated form performed for the apo form of IsdA-N did not reproduce the hydrogen bond between Y166 and Y170 observed in its crystal structure. Water molecules and charge-neutralizing ions were placed around each protein using Solvate version 1.0.[42] Water molecules were further added to the system with a thickness of more than 5 Å to form a box-shaped system using the LEaP module of AmberTools version 1.5.[43] The Amber ff99SB force field[44] was employed for the proteins, and the TIP3P model[45] was used for the water molecules.

The partial charges of deprotonated tyrosine and heme bound to deprotonated tyrosine or chloride ions were determined as follows. We first optimized the structures of the 4-methylphenoxide, heme 4-methylphenoxide, and heme chloride at the B3LYP/6-31G(d)[46,47] level using Gaussian 09.[48] The electrostatic potentials around the molecules were then calculated. The partial charges were determined to fit the electrostatic potentials using the restrained electrostatic potential (RESP) method,[49] implemented in the ANTECHAMBER module of AmberTools version 1.5. It is important to note that we used two different sets of partial charges for the apo and holo form simulations. Bond, angle, and torsion parameters describing the interaction between heme and deprotonated tyrosine were determined on the basis of the energy changes caused by small structural changes. The partial charges and parameters used here are described previously.[50]

Each MD simulation was performed as follows. First, the positions of the water molecules and the counterions were optimized by a 200-step energy minimization. The whole system was then subjected to a 200-step energy minimization. The system was heated gradually to 300 K in a 200 ps constant-*NVT* MD simulation with harmonic position restraints imposed on all heavy atoms of the solutes with a force constant of 10 kcal mol^{-1} Å^{-2}. During the subsequent 800 ps constant-*NPT* simulation, the restraints were gradually relaxed and the system was equilibrated at 300 K and 1.0 × 10^5 Pa. The SHAKE algorithm[51] was employed to constrain all bond lengths involving hydrogen atoms, which allowed the use of a time step of 2 fs. Electrostatic interactions were calculated using the particle mesh Ewald (PME) method,[52,53] with a cutoff radius of 8 Å. The temperature was controlled by the Langevin dynamics algorithm[54] with a collision frequency of 2.0 ps^{-1}. The pressure was controlled using the weak coupling method.[55] The minimization and equilibration runs were conducted using the Sander or PMEMD module of AMBER 11.[43]

A production run was conducted for 200 ns, maintaining the temperature at 300 K and the pressure at 1.0 × 10^5 Pa with GROMACS version 4.5.5.[56] The AMBER topology files were converted into the GROMACS format using the ffAmber script.[57] During the production run, the P-LINCS algorithm[58] was employed to constrain the bond lengths involving hydrogen atoms.

Calculation of Binding Free Energy using the MM−PB/SA Method. The molecular mechanics−Poisson−Boltzmann/surface area (MM−PB/SA)[59] method was employed to calculate the binding free energy, ΔG_{bind}, for the complexes between the NEAT domains and heme. Here, we considered the following reaction:

$$\text{protein} + \text{heme-Cl} \rightarrow \text{protein−heme} + \text{Cl}^-$$

where protein is IsdH-N3, IsdA-N, or IsdC-N and the tyrosine residue to which the heme iron binds is deprotonated in both the apo and holo forms. In the MM−PB/SA method, ΔG_{bind} was calculated as

Table 1. Results of the ITC Experiment with Isd Proteins and Metalloporphyrins[a]

metalloporphyrin	protein	$\Delta H°$ (kcal/mol)	$-T\Delta S°$ (kcal/mol)	$\Delta G°$ (kcal/mol)	K_d (nM)
heme	IsdH-N3	−10.6 ± 0.1	0.39	−10.2 ± 0.1	34 ± 8
	IsdA-N	−11.0 ± 0.1	0.30	−10.8 ± 0.1	14 ± 4
	IsdC	−14.6 ± 0.1	3.4	−11.2 ± 0.1	6.5 ± 1.4
Mn-PPIX	IsdH-N3	−5.77 ± 0.1	−2.84	−8.61 ± 0.1	490 ± 60
	IsdA-N	−9.5 ± 0.1	−1.8	−11.3 ± 0.2	5.7 ± 2.1
	IsdC	−14.6 ± 0.1	3.25	−11.4 ± 0.1	4.5 ± 1.0
Ga-PPIX	IsdH-N3	−7.67 ± 0.1	−1.97	−9.62 ± 0.1	91 ± 21
	IsdA-N	−8.0 ± 0.1	−3.0	−11.0 ± 0.2	34 ± 8
	IsdC	−13.2 ± 0.1	0.95	−12.2 ± 0.2	14 ± 4

[a]Temperature of 25 °C (298.15 K).

$$\Delta G_{bind} = E_{MM}(\text{protein–heme}) - TS(\text{protein–heme}) + \Delta G_{solv}(\text{protein–heme}) + E_{MM}(Cl^-) - TS(Cl^-) + \Delta G_{solv}(Cl^-) - [E_{MM}(\text{protein}) - TS(\text{protein}) + \Delta G_{solv}(\text{protein}) + E_{MM}(\text{heme-Cl}) - TS(\text{heme-Cl}) + \Delta G_{solv}(\text{heme-Cl})] + \Delta E_{corr}$$

where $E_{MM}(X)$ and $S(X)$ are molecular mechanical energy and entropy of X calculated in the gas phase, respectively, T is the temperature (298.15 K), $\Delta G_{solv}(X)$ is the solvation free energy, and ΔE_{corr} is a correction term. $E_{MM}(X)$ was calculated as the sum of the bond, angle, torsion, van der Waals, and electrostatic energies. The vibrational component of $S(X)$ was estimated by the quasi-harmonic approximation method.[60,61] $\Delta G_{solv}(X)$ was calculated as the sum of the polar $[\Delta G_{pol}(X)]$ and nonpolar $[\Delta G_{np}(X)]$ contributions, except for $\Delta G_{solv}(Cl^-)$, for which the experimental value (−74.7 kcal mol^{-1})[62] was used. $\Delta G_{pol}(X)$ was calculated by solving the Poisson–Boltzmann equation with interior and exterior dielectric constants of 1 and 80, respectively, with a salt concentration of 0.2 M. $\Delta G_{np}(X)$ was approximated using a linear function of the solvent accessible surface area (SASA) of solute X as

$$\Delta G_{np}(X) = \gamma \text{SASA} + b$$

where γ and b were 0.00542 kcal mol^{-1} Å^{-2} and 1.008 kcal mol^{-1}, respectively. The solvent probe radius used in the calculation of SASA was set at 1.4 Å. The correction term, ΔE_{corr}, was added to consider the energy change due to the cleavage and formation of the chemical bonds, which was calculated approximately as

$$\Delta E_{corr} = E_{QM}(\text{4MP–heme}) + E_{QM}(Cl^-) - [E_{QM}(\text{4MP}^-) + E_{QM}(\text{heme-Cl})] - \{E_{MM}(\text{4MP–heme}) + E_{MM}(Cl^-) - [E_{MM}(\text{4MP}^-) + E_{MM}(\text{heme-Cl})]\}$$

where $E_{QM}(X)$ is the quantum mechanical (QM) energy of X calculated at the B3LYP/6-31G(d) level and 4MP stands for 4-methylphenoxide.

In addition, we also calculated the polar contributions to ΔG_{solv}(protein–heme), ΔG_{solv}(protein), and ΔG_{solv}(heme-Cl) using a generalized Born (GB) model to decompose the energy changes into per-residue contributions.[63]

All the calculations were performed using the MD trajectories between 10 and 200 ns recorded every 20 ps (9500 snapshots for each protein).

Principal Component Analysis. Principal component analysis (PCA) was performed for the MD trajectories of the apo and holo forms of the wild-type IsdC-N protein and the IsdC-N-F130A mutant. The variance–covariance matrix was calculated from the Cα atom coordinates of the MD trajectories between 10 and 200 ns after superimposing them onto their average coordinates. The matrix was then diagonalized to obtain the principal component eigenvectors. Every structure in the MD trajectories was projected onto the space defined by the first and second principal component eigenvectors to graphically display the conformational distribution.

Cloning, Expression, Purification, and Binding Analysis of the Isd Mutants. To verify the predictions by the MD simulations, four mutants of full-length IsdC were prepared with a Takara Bio mutagenesis kit. A full-length IsdC-E88A mutant, the full-length IsdC-loop 1H chimera, and a full-length IsdC-F130A mutant were constructed using the pairs of primers described in Table S2 of the Supporting Information. A double mutant of the full-length loop 1H chimera and E88A (IsdC-E88A-loop 1H) was also constructed by combining the preceding primer sets. As a complementary approach, we also constructed an IsdH-N3-loop 1C chimera, whose loop 1 region (residues Phe-555–Glu-562) is substituted with the corresponding region (Tyr-39–Thr-46) of IsdC (Table S1 of the Supporting Information). Expression and purification were performed as described above.

The binding affinities of these mutants for heme were determined by ITC in the same manner described above. The concentration of full-length IsdC-E88A-loop 1H in the calorimeter cell was 12 μM.

Heme Transfer between Three Isd Mutants and IsdA. As IsdA (also IsdA-N) and the IsdC mutants were not well separated by ion-exchange chromatography, we used a size-exclusion chromatography column, HiLoad 16/60 Superdex 200 (GE Healthcare), to separate these two proteins (Figure S1 of the Supporting Information). Note that full-length IsdA was eluted from the column at the volume equivalent to that of a 100.3 kDa protein.[64] The holo form of full-length IsdC-F130A (16 μM) and the apo form of full-length IsdA (16 μM) were mixed in a 3.5 mL solution and then injected into the column and equilibrated with 50 mM Tris-HCl buffer (pH 8.0) containing 200 mM NaCl. Analyses of two heme transfers between the holo form of full-length IsdC-E88A-loop 1H and the apo form of full-length IsdA and between the holo form of IsdH-N3-loop 1C and the apo form of full-length IsdA were performed in a similar manner.

dx.doi.org/10.1021/bi4008325 | Biochemistry 2013, 52, 8866–8877

RESULTS AND DISCUSSION

Binding of Heme and Metalloporphyrins to NEAT Proteins. The thermodynamic parameters of the binding of heme or metalloporphyrins to the NEAT domains were determined by ITC (Table 1).

The injection of heme into protein solutions containing NEAT domains released a large amount of heat. As shown in Table 1, the magnitude of exothermic heat increased from IsdH-N3 (-10.6 ± 0.1 kcal mol^{-1}) to IsdA-N (-11.0 ± 0.1 kcal mol^{-1}) to IsdC (-14.6 ± 0.1 kcal mol^{-1}). The dissociation constant of IsdC was consistently the smallest ($K_d = 6.5 \pm 1.4$ nM), and therefore, it exhibited the strongest affinity for heme. The K_d of IsdA-N was intermediate (14 ± 4 nM), and that of IsdH-N3 was the largest (34 ± 8 nM). The order of affinities corresponded to the reported biological order of heme transport across the cell wall mediated by the NEAT domains. Interestingly, the difference in $\Delta H°$ between IsdA-N and IsdC was 3.6 kcal mol^{-1}, whereas that for $\Delta G°$ was only 0.4 kcal mol^{-1}, indicating a relatively larger entropy loss associated with the binding of heme to IsdC-N. This observation was consistent with a previous report that showed the heme-binding pocket of IsdC-N is flexible in the apo form and becomes rigid upon binding to heme.[65] The affinity of heme was 2−3-fold larger for IsdC than for IsdA. This value is smaller than that determined in a previous kinetic report (5−15-fold).[27] The discrepancy may be due to differences in experimental conditions (protein concentration or methods) and the binding by heme as a dimer in our ITC experiments. However, we note that the trend of affinities is consistent with the previous report.

We next measured the K_d values of Mn-PPIX and Ga-PPIX, two closely related analogues of heme.[38,66] The results of ITC indicated that all the metalloporphyrins tested bound to each of the three NEAT domains with similar affinities. Furthermore, the K_d values for Mn-PPIX and Ga-PPIX became smaller for the downstream NEAT domains, similar to the K_d for heme (Table 1). However, the differences in $\Delta G°$ and $\Delta H°$ related to the change in metal ion were not constant between the NEAT domains. Notably, the affinities of Mn-PPIX and Ga-PPIX were both lower than that of heme in the case of IsdH-N3 but higher in the cases of IsdA-N and IsdC. Although the ITC data were collected at 25 °C, we expect that the order of the affinities among the NEAT domains is not changed at 37 °C. To evaluate the temperature dependence of the affinity, we measured the affinity of IsdH-NEAT3 for heme in the temperature range from 15 to 30 °C. Although the affinity could not be measured at 37 °C because of the instability of the baseline of the ITC instrument, the K_d value remained almost constant, within experimental error, in this temperature range (Table S3 of the Supporting Information).

The stoichiometry indicated that two molecules of heme bind to IsdA-N and IsdC-N (Figure S2 of the Supporting Information), as previously explained for IsdH-N3.[50] The same stoichiometry was obtained from experiments using non-iron metalloporphyrins. Given that heme forms dimers in the high-concentration solutions employed for the ITC experiments, we believe that heme and the non-iron metalloporphyrins bind to the NEAT domains as dimers under the conditions used for the ITC experiment. The thermodynamic parameters obtained from the ITC measurements are affected little by the binding of the extra heme molecule because the second heme molecule binds very weakly to the heme−NEAT domain complex.[50]

Direct Transfer of Metalloporphyrin from IsdH-N3 to IsdC. Direct transfer of heme from IsdH-N3 to IsdC has been demonstrated by electrospray ionization mass spectrometry (ESI-MS).[26] In this study, we determined the direct transfer of metalloporphyrins from IsdH-N3 to IsdC using UV−visible spectroscopy. After incubation of holo-IsdH-N3 with full-length apo-IsdC for 2 min and subsequent separation on a DEAE ion-exchange column, the solution containing IsdH-N3 showed a marked decrease in the intensity of the Soret band. In contrast, the intensity of the Soret band of the IsdC sample increased markedly (Figure 2 and Figure S3 of the Supporting Information). These changes in the spectra closely resembled those observed in our previous experiments using IsdH-N3 and full-length IsdA,[38] indicating that metalloporphyrins were transferred effectively from IsdH-N3 to IsdC in the absence of the intermediary transporter IsdA-N. This rapid transfer also suggests that IsdH-N3 and IsdC form a heme-transfer intermediate complex like the IsdA−IsdC complex.[28] Meanwhile, back-transfer of metalloporphyrins from full-length holo-IsdC to apo-IsdH-N3 did not occur even after incubation for 20 min. These results suggest that the transfer of metalloporphyrin is controlled by thermodynamic equilibrium.

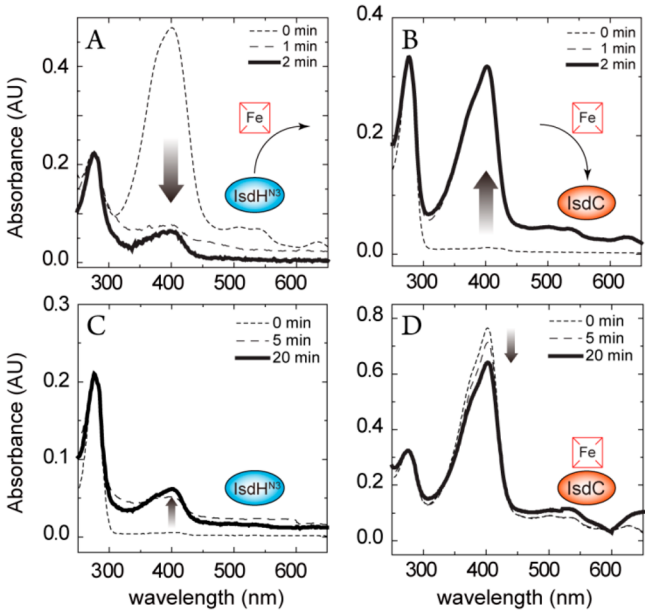

Figure 2. Transfer of heme between IsdH-N3 and IsdC. (A and C) IsdH-N3 spectra after elution from the DEAE column. (B and D) IsdC spectra. Heme bound to IsdH-N3 was effectively transferred to apo-IsdC (A and B), whereas heme bound to IsdC was not effectively transferred to apo-IsdH-N3 (C and D). The transfer of Mn-PPIX and Ga-PPX is shown in Figure S3 of the Supporting Information.

Theoretical Values of Binding Free Energies. We estimated the free energies of binding of heme to IsdH-N3, IsdA-N, and IsdC-N using the MM−PB/SA method. The correction term, ΔE_{corr}, was calculated to be -104.5 ± 2.0 kcal mol^{-1}. Calculated ΔG_{bind} values and their components are listed in Table 2. The sufficiency of conformation sampling was assessed by monitoring the time evolution of the first principal component in the form of the slowest mode of variation for each of the apo and holo forms of the three NEAT domains (Figure S4 of the Supporting Information). We found that the 200 ns MD simulations were sufficient to obtain convergent results for all except the apo form of IsdH-N3, where a

dx.doi.org/10.1021/bi4008325 | Biochemistry 2013, 52, 8866−8877

Table 2. Binding Free Energy and Energy Decomposition of ΔG Calculated by the MM−PB/SA Method (kilocalories per mole)[a]

contribution	IsdH-N3	IsdA-N	IsdC-N	IsdC-N-loop 1H
ΔE_{EEL}	172.08	−219.64	−133.83	26.95
ΔE_{vdw}	−37.72	−23.19	−43.51	−39.84
$\Delta E_{internal}$[b]	−2.53	−2.82	−7.05	1.90
ΔG_{PB}	−85.37	267.90	197.49	40.04
ΔG_{SA}	−3.64	−4.41	−3.94	−3.99
ΔG_{MMPBSA}[c]	42.82	17.84	9.16	25.06
$-T\Delta S_{solute}$	39.41	39.46	41.69	32.73
ΔE_{corr}[d]	−104.5	−104.5	−104.5	−104.5
ΔG	−22.3	−47.2	−53.6	−46.7

[a]These data were calculated from 9500 snapshots during a 200 ns production run. [b]The $\Delta E_{internal}$ term is a summation of ΔE_{bond}, ΔE_{angle}, and $\Delta E_{torsion}$. [c]ΔG_{MMPBSA} term is a summation of ΔE_{EEL}, ΔE_{vdw}, $\Delta E_{internal}$, ΔG_{PB}, and ΔG_{SA}. [d]ΔE_{corr} is a term to correct the MM energy between heme-binding Tyr and the iron in heme to QM energy.

conformation change was observed at 150 ns. Although the ΔG_{bind} values were overestimated compared with the ITC values, the order of affinity was completely consistent between these two techniques. ΔG_{bind} of IsdC-N was the smallest, and ΔG_{bind} of IsdH-N3 was the largest.

Comparison of the free energy components revealed differences in the interaction mechanism between the proteins. IsdH-N3 showed a positive average electrostatic energy change (ΔE_{elec} = 172.08 kcal mol^{-1}), whereas IsdA-N and IsdC-N showed negative values (−219.64 and −133.83 kcal mol^{-1}, respectively). This indicated that the electrostatic interaction between IsdH-N3 and heme was unfavorable (Table 2). Meanwhile, the change in the polar contribution to the solvation free energy, ΔG_{pol}, was negative (−85.37 kcal mol^{-1}) in IsdH-N3 and positive in IsdA-N and IsdC-N (267.90 and 197.49 kcal mol^{-1}, respectively). These results indicate that favorable electrostatic interactions are formed between IsdA-N or IsdC-N and heme, accompanying the desolvation of interface residues, whereas the electrostatic interactions between IsdH-N3 and heme are not very favorable.

To identify key residues for heme binding, ΔG_{bind} was decomposed into the contribution of each residue. We used the GB model instead of the PB method to calculate the polar contribution of the solvation free energies. The contributions of backbone and side chain atoms of each residue to ΔG_{bind} are plotted against residue number in Figure 3. On the basis of the comparison of the cumulative plots of these contributions (Figure 3E), we selected two interesting regions for further analysis that showed large differences in the values of ΔG_{bind} among the Isd proteins.

The first region was located near loop 1 between strand β1b and the 3_{10} helix (Figure 3A). In this region, IsdH-N3 displayed several residues with unfavorable contributions to the binding of heme, particularly Glu-556 and Glu-559 (Figure 3B), whereas IsdA-N and IsdC-N have fewer unfavorable residues (Figure 3C,D). As a result, the loop 1 region of IsdH-N3 was less suitable for binding heme than IsdA and IsdC. Although the primary sequence of this region varies among the NEAT domains as shown in their sequence alignment (Figure 1A), the serine residue at the end of loop 1 region is well-conserved. This serine residue forms a hydrogen bond with the propionate group of heme in the crystal structures of all the NEAT domains. However, MD simulations suggested that the strength

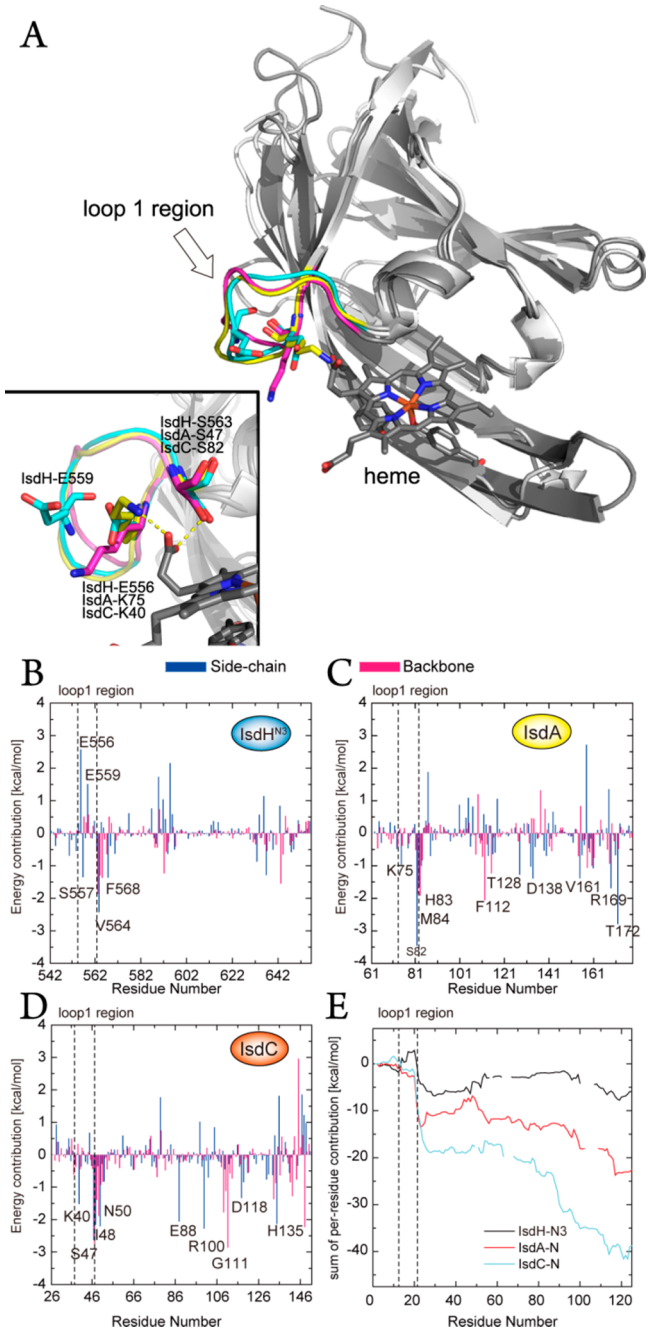

Figure 3. Per-residue binding free energy decomposition. (A) Superposition of structures of IsdH-N3 (blue), IsdA-N (yellow), and IsdC-N (red). (B−D) Energetic contributions of each residue in IsdH-N3, IsdA-N, and IsdC-N to the binding of heme, respectively. (E) Additive energies of each residue from the N-terminus. The loop 1 region is indicated by dashed lines in each panel.

of this hydrogen bond varied between the receptors. The plots of the time evolution of the hydrogen bond distances indicated that the hydrogen bond in IsdH-N3 was less stable than those in IsdA-N and IsdC-N (Figure 4A). Importantly, when the loop 1 region (residues 39−46) of IsdC-N was substituted with the corresponding region (residues 555−562) of IsdH-N3 (the IsdC-N-loop 1H chimera), the hydrogen bond became unstable like that of IsdH-N3 (Figure 4B). Consistent with this observation, the MM−PB/SA calculation for this chimera predicted that this substitution significantly reduced its affinity

dx.doi.org/10.1021/bi4008325 | Biochemistry 2013, 52, 8866−8877

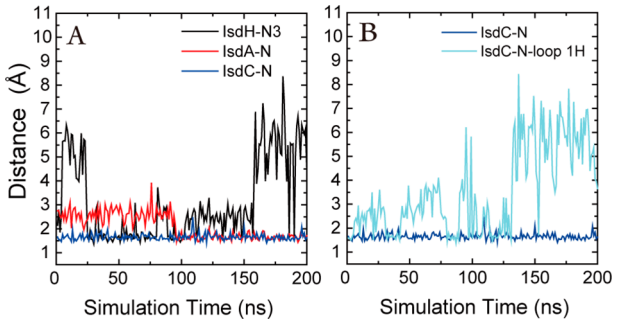

Figure 4. Plot of the distance between the conserved heme-binding serine residue and the proximal propionate of heme in the MD trajectories for 200 ns. (A) Comparison of wild-type Isd NEAT domains. Black, red, and blue traces depict data for IsdH-N3, IsdA-N, and IsdC-N, respectively. The hydrogen bond of IsdC-N remained completely intact during the simulation. (B) The IsdC-N-loop 1H mutant, whose loop 1 region was replaced with the IsdH-N3-type loop 1, showed a more fragile hydrogen bond (light blue).

for heme (Table 2). In addition, ΔE_{elec} and ΔG_{pol} were increased and decreased by the substitution, respectively, approaching the values of wild-type IsdH-N3 (Table 2). It is therefore proposed that the loop 1 region plays an important role in tuning the affinity of IsdH-N3 from those of IsdA-N and IsdC-N. This series of computational experiments demonstrates that an excess of negatively charged residues in the loop 1 region (four Glu residues) is detrimental to the binding affinity of IsdH-N3 compared with those of IsdA-N and IsdC-N (Figure 1A). The repulsive interaction between the glutamic acids and the propionate group of heme probably destabilizes the hydrogen bond and increases the unfavorable ΔE_{elec} component.

The second interesting region identified in our analysis was comprised of Glu-88 and Arg-100 of IsdC, which showed favorable contributions to ΔG_{bind} of IsdC (Figure 3D). These residues formed a stable salt bridge in the MD simulation of the holo form of IsdC-N. In contrast, the salt bridge was unstable in the MD simulation of the apo form (Figure S5 of the Supporting Information), despite a long separation between these residues and the heme-binding pocket. Sequence alignment indicated that Glu88 is unique to IsdC-N, whereas Arg100 is conserved in all the NEAT domains (Figure 1A). We therefore predicted that the pair of Glu-88 and Arg-100 is important for the enhanced affinity of IsdC-N with respect to IsdA-N. The replacement of Glu-88 of IsdC-N with Ala would significantly decrease its affinity for heme.

Characterization of Chimeric and Mutant Proteins. To verify the predictions made from the MD simulations, we measured $\Delta H°$ and $\Delta G°$ for binding of heme to IsdC-loop 1H by ITC. $\Delta H°$ of the chimeric protein was 1.9 kcal mol^{-1} weaker than that of the wild type (Table 3). This observation was consistent with the prediction made from the MD simulation. The affinity was also weaker for the chimeric construct ($\Delta\Delta G°$ = 0.7 kcal mol^{-1}). Next, we examined the effects of the E88A mutation of wild-type IsdC and the combined mutation with the IsdC-loop 1H construct using ITC. In agreement with the prediction of the MD simulation, we found that the E88A mutations increased $\Delta H°$ by 3.4 kcal mol^{-1} (from −14.6 to −11.2 kcal mol^{-1}) and 3.6 kcal mol^{-1} (from −12.7 to −9.1 kcal mol^{-1}) for the wild-type and chimera proteins, respectively (Table 3). In addition, this result indicated that the energetic effect of loop 1 and E88 on enthalpy was additive within acceptable margins of error. However, the increases in free energy were small for all the chimeric and mutant proteins [$\Delta\Delta G°$ = 0.7−0.9 kcal mol^{-1} (Table 3)]. This was probably due to the enthalpy−entropy compensation effect.[67,68] When the interaction was not very favorable, the amino acids or the functional groups of the ligand in the binding interface remained flexible, which reduced the magnitude of the entropy loss upon binding.

We measured the affinity of IsdH-N3-loop 1C in the same manner to determine whether the effect of the loop 1 region is reversible. The $\Delta H°$ and $\Delta G°$ values of this protein decreased by 0.7 and 1.1 kcal mol^{-1}, respectively, from those of the wild type (Table 3). The results for IsdC-loop 1H and IsdH-loop 1C clearly indicate that the affinity of the Isd-NEAT domains for heme (and other metalloporphyrins) is influenced by the loop region.

Role of F130 of IsdC. Phenylalanine 130 (F130) of IsdC is in the proximity of Y132, the tyrosine residue that is coordinated to the iron atom of heme. Sequence alignment indicates that this phenylalanine is unique to IsdC. Other NEAT domains have an isoleucine residue at the corresponding position (Figure 1A). We constructed a model of the F130I mutant of IsdC-N (IsdC-N-F130I) and performed MD simulations to investigate the role of this residue in heme binding.

Comparison of the MD trajectories between the wild-type and mutant IsdC-N proteins indicates that the F130I mutation destabilized the hydrogen bond formed between the Oη atoms of Y132 and Y136 in the apo form (Figure 5). The distance between the two atoms was <3.5 Å for 96% of the simulation time in the MD simulation of the apo form of wild-type IsdC-N (Figure 5). In the apo form of wild-type IsdA-N, the corresponding hydrogen bond formed between Y166 and Y170 was also stably maintained for 99% of the simulation time. However, the probability of hydrogen bond formation decreased to 82% in the MD simulation of the apo form of IsdC-N-F130I (Figure 5). F130, Y132, and Y136 of IsdC and

Table 3. Results of the ITC Experiment with the Isd Proteins and Heme[a]

protein	$\Delta H°$ (kcal/mol)	$-T\Delta S°$ (kcal/mol)	$\Delta G°$ (kcal/mol)	K_d (nM)
IsdC-WT	−14.6 ± 0.1	3.4	−11.2 ± 0.1	6.5 ± 1.4
IsdC-loop 1H	−12.7 ± 0.1	2.2	−10.5 ± 0.2	21 ± 7
IsdC-E88A	−11.2 ± 0.1	0.70	−10.5 ± 0.2	23 ± 9
IsdC-E88A-loop 1H	−9.1 ± 0.1	−1.3	−10.4 ± 0.1	23 ± 4
IsdC-F130A	−14.4 ± 0.1	4.2	−10.2 ± 0.1	32 ± 6
IsdH-N3	−10.6 ± 0.1	0.39	−10.2 ± 0.1	34 ± 8
IsdH-N3-loop 1C	−11.3 ± 0.1	−0.11	−11.3 ± 0.1	5.4 ± 2.2

[a]Temperature of 25 °C (298.15 K).

dx.doi.org/10.1021/bi4008325 | *Biochemistry* 2013, 52, 8866−8877

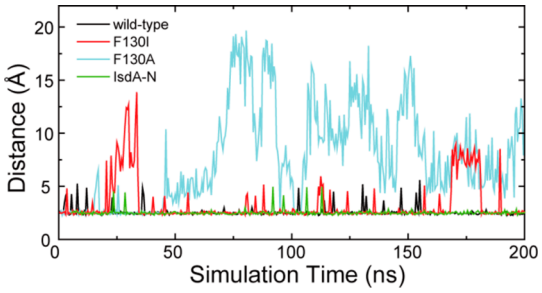

Figure 5. Plot of the distance between the oxygen atoms of Y132 and Y136 of IsdC in the MD trajectories for 200 ns. Black, red, light blue, and green traces depict data for wild-type IsdC-N, IsdC-N-F130I, IsdC-N-F130A, and IsdA-N, respectively.

I164, Y166, and Y170 of IsdA are located in β8, which forms a β-hairpin structure with β7 (hereafter termed the β7−β8 hairpin). F130 of IsdC-N makes a hydrophobic contact with I121 located in β7 (Figure S6 of the Supporting Information). Similarly, I164 of IsdA-N makes a hydrophobic contact with V161 (Figure S6 of the Supporting Information). The β7−β8 hairpin was the most variable part in each NEAT domain structure in the apo form. Given that the β7−β8 hairpin of apo-IsdC-N-F130I showed a variation larger than that of the wild type (Figure 6A,C), the increased mobility of the β7−β8 hairpin may be responsible for the destabilization of the hydrogen bond. The β7−β8 hairpin of IsdC is longer than that of IsdA. Thus, a residue more bulky than isoleucine, such as phenylalanine, may be necessary to suppress the mobility of the β7−β8 hairpin of IsdC.

To verify the hypothesis described above, we made a model of the F130A mutant of IsdC-N (IsdC-N-F130A) and performed MD simulations of this mutant. As expected, the probability of hydrogen bond formation between Y132 and Y136 in the apo form decreased to 23% (Figure 5) and the mobility of the β7−β8 hairpin was further enhanced (Figure 6A,C,E). In contrast, the hydrogen bond between the two tyrosine residues was maintained in the holo form of IsdC-N-F130A throughout the simulation, as seen for the holo forms of wild-type and IsdC-N-F130I proteins. The variation of the β7−β8 hairpin of the holo form of IsdC-N-F130A was as small as that of the holo forms of the wild-type and IsdC-N-F130I proteins (Figure 6B,D,F). We accordingly expected that the affinity of IsdC-N-F130A for heme would be weaker than that of the wild type, because of the larger loss of binding entropy.

Next, we experimentally verified the prediction for IsdC-N-F130A using ITC (Table 3 and Figure S7 of the Supporting Information). The $-T\Delta S^\circ$ term increased by 0.8 kcal mol^{-1}, reflecting the larger entropy loss expected for IsdC-N-F130A. Interestingly, ΔH° also increased by 0.2 kcal mol^{-1}, leading to a further decrease in binding affinity ($\Delta\Delta G$ = 1.0 kcal mol^{-1}). The increase in ΔH° was explained by the per-residue contribution of F130 to ΔH of wild-type IsdC [0.5 kcal mol^{-1} (Figure 3D)]. Unlike the case for the wild type, it is possible that Y132 of IsdC-N-F130 was protonated in the apo form, because of the loss of the hydrogen bond with Y136, which may lower the energy of the apo form causing an increase in ΔH°.

The β7−β8 hairpin of IsdC-N is six residues longer than those of IsdH-N3 and IsdA-N. We have demonstrated previously that the longer β7−β8 hairpin is necessary for transferring heme to IsdE.[29] The longer β7−β8 hairpin could cause a larger entropy loss upon binding to heme, which would

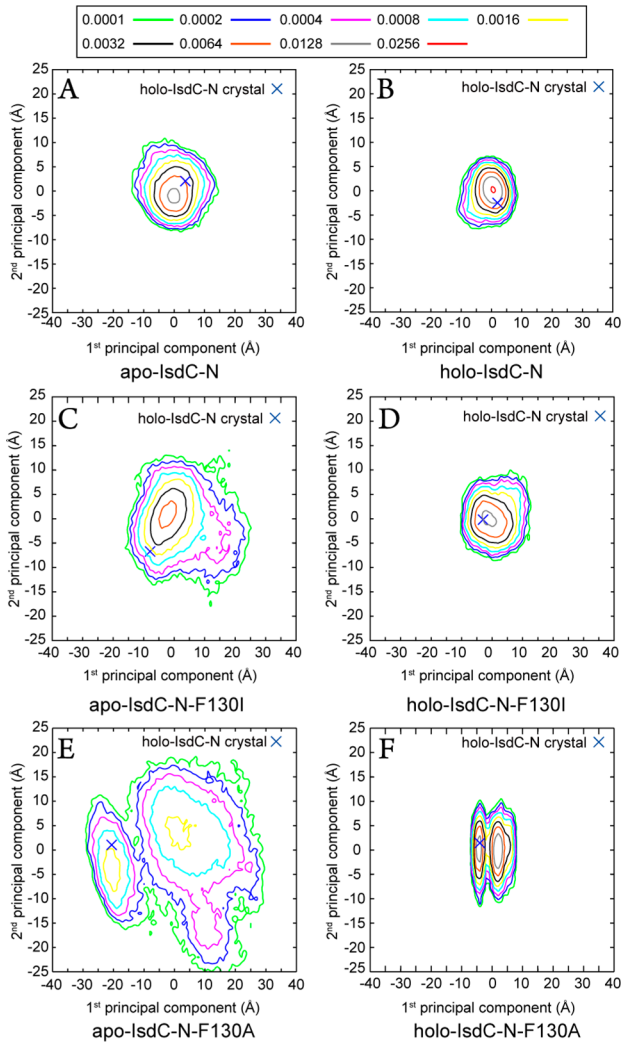

Figure 6. Projections of conformational ensembles of the β7−β8 hairpin onto the space defined by the first and second principal axes derived from MD simulations for apo-IsdC-N (A), holo-IsdC-N (B), apo-IsdC-N-F130I (C), holo-IsdC-N-F130I (D), apo-IsdC-N-F130A (E), and holo-IsdC-N-F130A (F). The x and y values represent the deviation from the average structure along the first and second principal axes, respectively, in angstroms. The positions of the crystal structure of IsdC in complex with heme (PDB entry 2O6P) are indicated by blue crosses.

weaken the affinity for heme and would be unfavorable for the final step of the heme-transfer pathway mediated by the NEAT domains. IsdC-N overcomes this potential hurdle by having a phenylalanine residue at position 130 and keeping the structure of the long hairpin rigid in the ligand-free form, along with a ΔH° support from the pair of Glu-88 and Arg-100.

Reversal of the Direction of Heme Transfer Using the Isd Mutants. We have shown above that the NEAT domain of Isd proteins located downstream in the heme-transfer pathway had a higher affinity for metalloporphyrins than for proteins located upstream. This suggests that the transfer of metalloporphyrin is driven by free energy. To confirm this hypothesis, we attempted to reverse the direction of the heme transfer by controlling the affinity of the NEAT domain for heme. As shown in Table 3, the affinities of IsdC mutants for heme were lower than that of IsdA-N. Therefore, we examined whether transfer of heme occurred from the holo

dx.doi.org/10.1021/bi4008325 | Biochemistry 2013, 52, 8866−8877

form of some of the IsdC mutants to the apo form of IsdA. The results demonstrated clearly that heme bound to the IsdC mutants was transferred effectively to apo-IsdA (Figure 7).

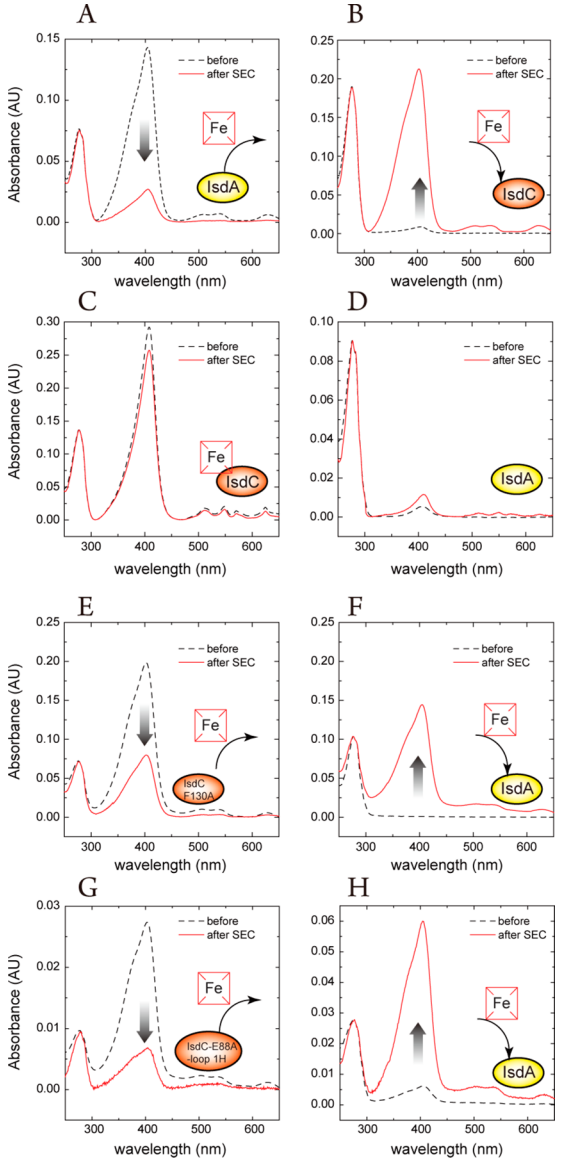

Figure 7. Transfer of heme between IsdA and IsdC and its mutants. (A, C, E, and G) Spectra of holo-Isd proteins (heme donor) and (B, D, F, and H) spectra of apo-Isd proteins (heme acceptor). The black lines represent the spectra after separation of the proteins by size-exclusion chromatography. In panels A and B, the amount of heme bound to wild-type IsdA decreased after incubation with IsdC. In panels C and D, heme bound to wild-type IsdC was not transferred effectively to wild-type IsdA. In panels E and F, heme bound to IsdC-F130A was transferred to wild-type IsdA. In panels G and H, heme bound to IsdC-E88A-loop 1H was also transferred to IsdA.

Under the same experimental conditions, wild-type IsdC did not transfer heme to IsdA (Figure 7). To the best of our knowledge, this is the first example among NEAT transporters in which heme is transferred in the reverse direction. Importantly, heme bound to the IsdH-N3-loop 1C chimera, whose affinity exceeds that of IsdA, was not transferred to IsdA (Figure S8 of the Supporting Information), in contrast to the experiment with wild-type IsdH-N3.[38] Therefore, we concluded that the direction of heme transfer is determined by the strength of the affinity between the NEAT domain and the metalloporphyrins.

Estimation of the Affinities of NEAT Domains of Other Bacteria. Recently, novel Isd-like proteins have been discovered in other important pathogens such as *Listeria monocytogenes*,[69,70] *Staphylococcus lugdunensis*,[71] *Bacillus cereus*, and *Bacillus anthracis*. In *B. anthracis*, BslK,[72] IsdX1, IsdX2, IsdC, and Hal (BAS0520)[73] are characterized as heme-binding and/or heme-transfer proteins. Sequence alignment of these proteins (Figure S9 of the Supporting Information) and the crystal structures of IsdX1[74] and IsdX2-NEAT5[75] suggest that the amino acid residues in loop 1 may influence the affinity for heme by changing the stability of the hydrogen bond between the conserved serine residue at the end of the loop and the propionate group of heme, as in the case of the NEAT domains of *S. aureus* (Figure S10 of the Supporting Information). According to our theoretical and experimental results, the NEAT domain displaying more negatively charged residues in loop 1 will exhibit a lower affinity for heme. In agreement with this expectation, IsdX1 of *B. anthracis*, which has three negatively charged residues in loop 1, exhibited a lower affinity for heme than BslK and IsdC, which have two negatively charged residues.[72] Therefore, we can estimate the affinity of experimentally uncharacterized NEAT domains on the basis of the number of negatively charged residues in loop 1. For example, Hal (Bas0520) of *B. anthracis* is estimated to have a lower affinity than the other NEAT domains of this pathogen because it has four negatively charged residues. Residues outside loop 1 can also affect the affinity for heme for some proteins, as shown for IsdC-N of *S. aureus*. Prediction of the affinities solely from the sequence data will therefore be difficult for these proteins. However, as we have demonstrated in this study, if precise tertiary structural models are available, it will be possible to estimate their affinities and to identify the critical binding residues based on MD simulations.

CONCLUSIONS

We have demonstrated using ITC that the affinity for heme and non-iron metalloporphyrins increases from IsdH-N3 to IsdA-N to IsdC, which is consistent with the sequence of events during heme transfer *in vitro*. On the basis of MD simulations, loop 1 and the pair of Glu-88 and Arg-100 unique to IsdC were predicted to be important for specifying the affinity order of NEAT transporters. In addition, F130, which is unique to IsdC-N, stabilized the longer $\beta7-\beta8$ hairpin of IsdC in the apo form, thus reducing the loss of entropy upon heme binding. All these predictions were verified using calorimetric techniques with IsdC mutant proteins, such as the IsdC-loop 1H chimera, the IsdC-E88A mutant, the IsdC-E88A-loop 1H chimera, and the IsdC-F130A mutant. In addition, we have shown that the IsdC-E88A-loop 1H chimera and the IsdC-F130A mutant, which displayed a lower affinity for heme than IsdA-N did, transferred heme back to IsdA. Because none of these key residues directly interact with the metal ion in metalloporphyrin, the order of affinity will not be changed by the type of central metal ion, as was partly demonstrated by the experiments using Mn-PPIX and Ga-PPIX. It is therefore expected that non-iron metalloporphyrins capable of binding to the NEAT domains will also be transferred by the NEAT domains into the pathogenic cells and will act as a molecular "Trojan horse" that disrupts the iron utilization pathway in the cells.

dx.doi.org/10.1021/bi4008325 | *Biochemistry* 2013, 52, 8866−8877

■ ASSOCIATED CONTENT

Supporting Information

Additional information about the experimental procedures, figures showing the transfer of metalloporphyrins and the binding isotherm determined by ITC, time evolution of the distance between Glu-88 and Arg-100, and multiple-sequence alignment of NEAT domains. This material is available free of charge via the Internet at http://pubs.acs.org.

■ AUTHOR INFORMATION

Corresponding Author

*Telephone: +81-3-5841-5455. Fax: +81-3-5841-8002. E-mail: virgospica93@bi.a.u-tokyo.ac.jp.

Funding

This work was supported by Grant-in-Aid for JSPS Fellows 25·6526. This work was supported, in part, by the Platform for Drug Discovery, Informatics, and Structural Life Science from the Ministry of Education, Culture, Sports, Science and Technology, Japan.

Notes

The authors declare no competing financial interest.

■ ACKNOWLEDGMENTS

The supercomputing resource was provided by the Human Genome Center, Institute of Medical Science, The University of Tokyo. We thank Enago (http://www.enago.jp) for the English language review.

■ ABBREVIATIONS

Isd, iron-regulated surface determinant; NEAT, near transporter; ITC, isothermal titration calorimetry; SEC, size-exclusion chromatography; PPIX, protoporphyrin IX; DMSO, dimethyl sulfoxide; DEAE, diethylaminoethyl; PDB, Protein Data Bank.

■ REFERENCES

(1) Trivier, D., and Courcol, R. J. (1996) Iron depletion and virulence in *Staphylococcus aureus*. *FEMS Microbiol. Lett. 141*, 117−127.

(2) Skaar, E. P. (2010) The Battle for Iron between Bacterial Pathogens and Their Vertebrate Hosts. *PLoS Pathog. 6*, e1000949.

(3) Haley, K. P., and Skaar, E. P. (2012) A battle for iron: Host sequestration and *Staphylococcus aureus* acquisition. *Microbes Infect. 14*, 217−227.

(4) Lowy, F. D. (2011) How *Staphylococcus aureus* Adapts to Its Host. *N. Engl. J. Med. 364*, 1987−1990.

(5) Radtke, A. L., and O'Riordan, M. X. D. (2006) Intracellular innate resistance to bacterial pathogens. *Cell. Microbiol. 8*, 1720−1729.

(6) Ratledge, C., and Dover, L. G. (2000) Iron metabolism in pathogenic bacteria. *Annu. Rev. Microbiol. 54*, 881−941.

(7) Klebba, P. E., Charbit, A., Xiao, Q., Jiang, X., and Newton, S. M. (2012) Mechanisms of iron and haem transport by *Listeria monocytogenes*. *Mol. Membr. Biol. 29*, 69−86.

(8) Haley, K. P., Janson, E. M., Heilbronner, S., Foster, T. J., and Skaar, E. P. (2011) *Staphylococcus lugdunensis* IsdG Liberates Iron from Host Heme. *J. Bacteriol. 193*, 4749−4757.

(9) Daou, N., Buisson, C., Gohar, M., Vidic, J., Bierne, H., Kallassy, M., Lereclus, D., and Nielsen-LeRoux, C. (2009) IlsA, a unique surface protein of *Bacillus cereus* required for iron acquisition from heme, hemoglobin and ferritin. *PLoS Pathog. 5*, e1000675.

(10) Mazmanian, S. K., Skaar, E. P., Gaspar, A. H., Humayun, M., Gornicki, P., Jelenska, J., Joachmiak, A., Missiakas, D. M., and Schneewind, O. (2003) Passage of heme-iron across the envelope of *Staphylococcus aureus*. *Science 299*, 906−909.

(11) Maresso, A. W., Garufi, G., and Schneewind, O. (2008) *Bacillus anthracis* secretes proteins that mediate heme acquisition from hemoglobin. *PLoS Pathog. 4*, e1000132.

(12) Gat, O., Zaide, G., Inbar, I., Grosfeld, H., Chitlaru, T., Levy, H., and Shafferman, A. (2008) Characterization of *Bacillus anthracis* iron-regulated surface determinant (Isd) proteins containing NEAT domains. *Mol. Microbiol. 70*, 983−999.

(13) Maresso, A. W., Chapa, T. J., and Schneewind, O. (2006) Surface protein IsdC and sortase B are required for heme-iron scavenging of *Bacillus anthracis*. *J. Bacteriol. 188*, 8145−8152.

(14) Grigg, J. C., Ukpabi, G., Gaudin, C. F. M., and Murphy, M. E. P. (2010) Structural biology of heme binding in the *Staphylococcus aureus* Isd system. *J. Inorg. Biochem. 104*, 341−348.

(15) Tiedemann, M. T., Muryoi, N., Heinrichs, D. E., and Stillman, M. J. (2008) Iron acquisition by the haem-binding Isd proteins in Staphylococcus aureus: Studies of the mechanism using magnetic circular dichroism. *Biochem. Soc. Trans. 36*, 1138−1143.

(16) Zhu, H., Xie, G., Liu, M., Olson, J. S., Fabian, M., Dooley, D. M., and Lei, B. (2008) Pathway for heme uptake from human methemoglobin by the iron-regulated surface determinants system of *Staphylococcus aureus*. *J. Biol. Chem. 283*, 18450−18460.

(17) Pilpa, R. M., Robson, S. A., Villareal, V. A., Wong, M. L., Phillips, M., and Clubb, R. T. (2009) Functionally Distinct NEAT (NEAr Transporter) Domains within the *Staphylococcus aureus* IsdH/HarA protein extract heme from methemoglobin. *J. Biol. Chem. 284*, 1166−1176.

(18) Spirig, T., Malmirchegini, G. R., Zhang, J., Robson, S. A., Sjodt, M., Liu, M., Kumar, K. K., Dickson, C. F., Gell, D. A., Lei, B., Loo, J. A., and Clubb, R. T. (2013) *Staphylococcus aureus* uses a novel multidomain receptor to break apart human hemoglobin and steal its heme. *J. Biol. Chem. 288*, 1065−1078.

(19) Pilpa, R. M., Fadeev, E. A., Villareal, V. A., Wong, M. L., Phillips, M., and Clubb, R. T. (2006) Solution structure of the NEAT (NEAr Transporter) domain from IsdH/HarA: The human hemoglobin receptor in *Staphylococcus aureus*. *J. Mol. Biol. 360*, 435−447.

(20) Dryla, A., Gelbmann, D., von Gabain, A., and Nagy, E. (2003) Identification of a novel iron regulated staphylococcal surface protein with haptoglobin-haemoglobin binding activity. *Mol. Microbiol. 49*, 37−53.

(21) Tiedemann, M. T., Heinrichs, D. E., and Stillman, M. J. (2012) Multiprotein heme shuttle pathway in *Staphylococcus aureus*: Iron-regulated surface determinant cog-wheel kinetics. *J. Am. Chem. Soc. 134*, 16578−16585.

(22) Mack, J., Vermeiren, C., Heinrichs, D. E., and Stillman, M. J. (2004) In vivo heme scavenging by *Staphylococcus aureus* IsdC and IsdE proteins. *Biochem. Biophys. Res. Commun. 320*, 781−788.

(23) Skaar, E. P., Gaspar, A. H., and Schneewind, O. (2004) IsdG and IsdI, heme-degrading enzymes in the cytoplasm of *Staphylococcus aureus*. *J. Biol. Chem. 279*, 436−443.

(24) Lee, W. C., Reniere, M. L., Skaar, E. P., and Murphy, M. E. P. (2008) Ruffling of Metalloporphyrins Bound to IsdG and IsdI, Two Heme-degrading Enzymes in *Staphylococcus aureus*. *J. Biol. Chem. 283*, 30957−30963.

(25) Reniere, M. L., Ukpabi, G. N., Harry, S. R., Stec, D. F., Krull, R., Wright, D. W., Bachmann, B. O., Murphy, M. E., and Skaar, E. P. (2010) The IsdG-family of haem oxygenases degrades haem to a novel chromophore. *Mol. Microbiol. 75*, 1529−1538.

(26) Muryoi, N., Tiedemann, M. T., Pluym, M., Cheung, J., Heinrichs, D. E., and Stillman, M. J. (2008) Demonstration of the iron-regulated surface determinant (Isd) heme transfer pathway in *Staphylococcus aureus*. *J. Biol. Chem. 283*, 28125−28136.

(27) Liu, M., Tanaka, W. N., Zhu, H., Xie, G., Dooley, D. M., and Lei, B. (2008) Direct hemin transfer from IsdA to IsdC in the iron-regulated surface determinant (Isd) heme acquisition system of *Staphylococcus aureus*. *J. Biol. Chem. 283*, 6668−6676.

(28) Villareal, V. A., Spirig, T., Robson, S. A., Liu, M., Lei, B., and Clubb, R. T. (2011) Transient weak protein−protein complexes transfer heme across the cell wall of *Staphylococcus aureus*. *J. Am. Chem. Soc. 133*, 14176−14179.

(29) Abe, R., Caaveiro, J. M. M., Kozuka-Hata, H., Oyama, M., and Tsumoto, K. (2012) Mapping ultra-weak protein−protein interactions between heme transporters of *Staphylococcus aureus*. *J. Biol. Chem. 287*, 16477−16487.
(30) Gupta, R. S. (1998) Protein phylogenies and signature sequences: A reappraisal of evolutionary relationships among archaebacteria, eubacteria, and eukaryotes. *Microbiol. Mol. Biol. Rev. 62*, 1435−1491.
(31) Waterhouse, A. M., Procter, J. B., Martin, D. M. A., Clamp, M., and Barton, G. J. (2009) Jalview Version 2: A multiple sequence alignment editor and analysis workbench. *Bioinformatics 25*, 1189−1191.
(32) Notredame, C., Higgins, D. G., and Heringa, J. (2000) T-Coffee: A novel method for fast and accurate multiple sequence alignment. *J. Mol. Biol. 302*, 205−217.
(33) Watanabe, M., Tanaka, Y., Suenaga, A., Kuroda, M., Yao, M., Watanabe, N., Arisaka, F., Ohta, T., Tanaka, I., and Tsumoto, K. (2008) Structural basis for multimeric heme complexation through a specific protein−heme interaction: The case of the third neat domain of IsdH from *Staphylococcus aureus*. *J. Biol. Chem. 283*, 28649−28659.
(34) Gaudin, C. F. M., Grigg, J. C., Arrieta, A. L., and Murphy, M. E. P. (2011) Unique Heme-Iron Coordination by the Hemoglobin Receptor IsdB of *Staphylococcus aureus*. *Biochemistry 50*, 5443−5452.
(35) Grigg, J. C., Vermeiren, C. L., Heinrichs, D. E., and Murphy, M. E. P. (2007) Haem recognition by a *Staphylococcus aureus* NEAT domain. *Mol. Microbiol. 63*, 139−149.
(36) Sharp, K. H., Schneider, S., Cockayne, A., and Paoli, M. (2007) Crystal structure of the heme-IsdC complex, the central conduit of the isd iron/heme uptake system in *Staphylococcus aureus*. *J. Biol. Chem. 282*, 10625−10631.
(37) Nakae, Y., Fukusaki, E. I., Kajiyama, S., Kobayashi, A., Nakajima, S., and Sakata, I. (2005) The convenient screening method using albumin for the tumor localizing property of Ga-porphyrin complexes. *J. Photochem. Photobiol., A 172*, 55−61.
(38) Moriwaki, Y., Caaveiro, J. M. M., Tanaka, Y., Tsutsumi, H., Hamachi, I., and Tsumoto, K. (2011) Molecular basis of recognition of antibacterial porphyrins by heme-transporter IsdH-NEAT3 of *Staphylococcus aureus*. *Biochemistry 50*, 7311−7320.
(39) Li, J. M., Umanoff, H., Proenca, R., Russell, C. S., and Cosloy, S. D. (1988) Cloning of the *Escherichia coli* K-12 hemB gene. *J. Bacteriol. 170*, 1021−1025.
(40) *The PyMol Molecular Graphics System*, version 1.5.0.3 (2010) Schrödinger, LLC, Portland, OR.
(41) Olsson, M. H. M., Sondergaard, C. R., Rostkowski, M., and Jensen, J. H. (2011) PROPKA3: Consistent Treatment of Internal and Surface Residues in Empirical pK_a Predictions. *J. Chem. Theory Comput. 7*, 525−537.
(42) Grubmüller, H. (1996) *SOLVATE*, version 1.0, Theoretical Biophysics Group, Institute for Medical Optics, Ludwig-Maximilians University, Munich.
(43) Case, D. A., Darden, T. A., Cheatham, T. E., III, Simmerling, C. L., Wang, J., Duke, R. E., Luo, R., Walker, R. C., Zhang, W., Merz, K. M., et al. (2010) *AMBER 11*, University of California, San Francisco.
(44) Hornak, V., Abel, R., Okur, A., Strockbine, B., Roitberg, A., and Simmerling, C. (2006) Comparison of multiple amber force fields and development of improved protein backbone parameters. *Proteins: Struct., Funct., Bioinf. 65*, 712−725.
(45) Jorgensen, W. L., Chandrasekhar, J., Madura, J. D., Impey, R. W., and Klein, M. L. (1983) Comparison of simple potential functions for simulating liquid water. *J. Chem. Phys. 79*, 926−935.
(46) Becke, A. D. (1993) Density-functional thermochemistry. III. The role of exact exchange. *J. Chem. Phys. 98*, 5648−5652.
(47) Lee, C. T., Yang, W. T., and Parr, R. G. (1988) Development of the Colle-Salvetti correlation-energy formula into a functional of the electron density. *Phys. Rev. B 37*, 785−789.
(48) Frisch, M. J., Trucks, G. W., Schlegel, H. B., Scuseria, G. E., Robb, M. A., Cheeseman, J. R., Scalmani, G., Barone, V., Mennucci, B., Petersson, G. A., Nakatsuji, H., Caricato, M., Li, X., Hratchian, H. P., Izmaylov, A. F., Bloino, J., Zheng, G., Sonnenberg, J. L., Hada, M., Ehara, M., Toyota, K., Fukuda, R., Hasegawa, J., Ishida, M., Nakajima, T., Honda, Y., Kitao, O., Nakai, H., Vreven, T., Montgomery, J. A., Jr., Peralta, J. E., Ogliaro, F., Bearpark, M., Heyd, J. J., Brothers, E., Kudin, K. N., Staroverov, V. N., Kobayashi, R., Normand, J., Raghavachari, K., Rendell, A., Burant, J. C., Iyengar, S. S., Tomasi, J., Cossi, M., Rega, N., Millam, J. M., Klene, M., Knox, J. E., Cross, J. B., Bakken, V., Adamo, C., Jaramillo, J., Gomperts, R., Stratmann, R. E., Yazyev, O., Austin, A. J., Cammi, R., Pomelli, C., Ochterski, J. W., Martin, R. L., Morokuma, K., Zakrzewski, V. G., Voth, G. A., Salvador, P., Dannenberg, J. J., Dapprich, S., Daniels, A. D., Farkas, Ö., Foresman, J. B., Ortiz, J. V., Cioslowski, J., and Fox, D. J. (2009) *Gaussian 09*, revision A.02, Gaussian, Inc., Wallingford, CT.
(49) Bayly, C. I., Cieplak, P., Cornell, W. D., and Kollman, P. A. (1993) A well-behaved electrostatic potential based method using charge restraints for deriving atomic charges: The RESP model. *J. Phys. Chem. 97*, 10269−10280.
(50) Vu, N. T., Moriwaki, Y., Caaveiro, J. M. M., Tsutsumi, H., Hamachi, I., Shimizu, K., and Tsumoto, K. (2013) Selective binding of antimicrobial porphyrins to the heme-receptor IsdH-NEAT3 of *Staphylococcus aureus*. *Protein Sci. 22*, 942−953.
(51) Ryckaert, J. P., Ciccotti, G., and Berendsen, H. J. C. (1977) Numerical Integration of the Cartesian Equations of Motion of a System with Constraints: Molecular Dynamics of *n*-Alkanes. *J. Comput. Phys. 23*, 327−341.
(52) Essmann, U., Perera, L., Berkowitz, M. L., Darden, T., Lee, H., and Pedersen, L. G. (1995) A smooth particle mesh Ewald method. *J. Chem. Phys. 103*, 8577−8593.
(53) Darden, T., York, D., and Pedersen, L. (1993) Particle mesh Ewald: An *N* log(N) method for Ewald sums in large systems. *J. Chem. Phys. 98*, 10089−10092.
(54) Uberuaga, B. P., Anghel, M., and Voter, A. F. (2004) Synchronization of trajectories in canonical molecular-dynamics simulations: Observation, explanation, and exploitation. *J. Chem. Phys. 120*, 6363−6374.
(55) Berendsen, H. J. C., Postma, J. P. M., Vangunsteren, W. F., Dinola, A., and Haak, J. R. (1984) Molecular dynamics with coupling to an external bath. *J. Chem. Phys. 81*, 3684−3690.
(56) Hess, B., Kutzner, C., van der Spoel, D., and Lindahl, E. (2008) GROMACS 4: Algorithms for highly efficient, load-balanced, and scalable molecular simulation. *J. Chem. Theory Comput. 4*, 435−447.
(57) Mobley, D. L., Chodera, J. D., and Dill, K. A. (2006) On the use of orientational restraints and symmetry corrections in alchemical free energy calculations. *J. Chem. Phys. 125*, 084902.
(58) Hess, B. (2008) P-LINCS: A parallel linear constraint solver for molecular simulation. *J. Chem. Theory Comput. 4*, 116−122.
(59) Kollman, P. A., Massova, I., Reyes, C., Kuhn, B., Huo, S. H., Chong, L., Lee, M., Lee, T., Duan, Y., Wang, W., Donini, O., Cieplak, P., Srinivasan, J., Case, D. A., and Cheatham, T. E. (2000) Calculating structures and free energies of complex molecules: Combining molecular mechanics and continuum models. *Acc. Chem. Res. 33*, 889−897.
(60) Andricioaei, I., and Karplus, M. (2001) On the calculation of entropy from covariance matrices of the atomic fluctuations. *J. Chem. Phys. 115*, 6289−6292.
(61) Tidor, B., and Karplus, M. (1994) The contribution of vibrational entropy to molecular association: The dimerization of insulin. *J. Mol. Biol. 238*, 405−414.
(62) Pliego, J. R., and Riveros, J. M. (2000) New values for the absolute solvation free energy of univalent ions in aqueous solution. *Chem. Phys. Lett. 332*, 597−602.
(63) Gohlke, H., Kiel, C., and Case, D. A. (2003) Insights into protein−protein binding by binding free energy calculation and free energy decomposition for the Ras−Raf and Ras−RaIGDS complexes. *J. Mol. Biol. 330*, 891−913.
(64) Vermeiren, C. L., Pluym, M., Mack, J., Heinrichs, D. E., and Stillman, M. J. (2006) Characterization of the heme binding properties of *Staphylococcus aureus* IsdA. *Biochemistry 45*, 12867−12875.
(65) Villareal, V. A., Pilpa, R. M., Robson, S. A., Fadeev, E. A., and Clubb, R. T. (2008) The IsdC Protein from *Staphylococcus aureus* Uses

a Flexible Binding Pocket to Capture Heme. *J. Biol. Chem. 283*, 31591−31600.
(66) Tiedemann, M. T., Pinter, T. B. J., and Stillman, M. J. (2012) Insight into blocking heme transfer by exploiting molecular interactions in the core Isd heme transporters IsdA-NEAT, IsdC-NEAT, and IsdE of *Staphylococcus aureus*. *Metallomics 4*, 751−760.
(67) Baron, R., and McCammon, J. A. (2013) Molecular Recognition and Ligand Association. *Annu. Rev. Phys. Chem. 64*, 151−175.
(68) Boots, H. M. J., and Debokx, P. K. (1989) Theory of enthalpy−entropy compensation. *J. Phys. Chem. 93*, 8240−8243.
(69) Newton, S. M. C., Klebba, P. E., Raynaud, C., Shao, Y., Jiang, X. X., Dubail, I., Archer, C., Frehel, C., and Charbit, A. (2005) The svpA-srtB locus of *Listeria monocytogenes*: Fur-mediated iron regulation and effect on virulence. *Mol. Microbiol. 55*, 927−940.
(70) Xiao, Q., Jiang, X., Moore, K. J., Shao, Y., Pi, H., Dubail, I., Charbit, A., Newton, S. M., and Klebba, P. E. (2011) Sortase independent and dependent systems for acquisition of haem and haemoglobin in *Listeria monocytogenes*. *Mol. Microbiol. 80*, 1581−1597.
(71) Zapotoczna, M., Heilbronner, S., Speziale, P., and Foster, T. J. (2012) Iron-Regulated Surface Determinant (Isd) Proteins of *Staphylococcus lugdunensis*. *J. Bacteriol. 194*, 6453−6467.
(72) Tarlovsky, Y., Fabian, M., Solomaha, E., Honsa, E., Olson, J. S., and Maresso, A. W. (2010) A *Bacillus anthracis* S-Layer Homology Protein That Binds Heme and Mediates Heme Delivery to IsdC. *J. Bacteriol. 192*, 3503−3511.
(73) Balderas, M. A., Nobles, C. L., Honsa, E. S., Alicki, E. R., and Maresso, A. W. (2012) Hal Is a *Bacillus anthracis* Heme Acquisition Protein. *J. Bacteriol. 194*, 5513−5521.
(74) Ekworomadu, M. T., Poor, C. B., Owens, C. P., Balderas, M. A., Fabian, M., Olson, J. S., Murphy, F., Balkabasi, E., Honsa, E. S., He, C., Goulding, C. W., and Maresso, A. W. (2012) Differential Function of Lip Residues in the Mechanism and Biology of an Anthrax Hemophore. *PLoS Pathog. 8*, e1002559.
(75) Honsa, E. S., Owens, C. P., Goulding, C. W., and Maresso, A. W. (2013) The Near-iron Transporter (NEAT) Domains of the Anthrax Hemophore IsdX2 Require a Critical Glutamine to Extract Heme from Methemoglobin. *J. Biol. Chem. 288*, 8479−8490.